

R.-F. Lin^{1,2}, D. O’C. Starr², A. Lare³, T. M. Rickenbach⁴, and B. Demoz²

¹Goddard Earth Sciences and Technology Center, University of Maryland, Baltimore County, Baltimore, MD, USA

²Laboratory for Atmospheres, NASA/GSFC, Greenbelt, MD, USA

³L-3 Communications Government Services, Inc., USA

⁴Department of Meteorology, San Jose State University, CA, USA

1. INTRODUCTION

The dissipation of cirrus anvil clouds is still not well understood by the community. To numerically simulate a full lifecycle of a cirrus anvil, one needs a domain large enough to encompass the entire cloud system, which can easily approach hundreds of kilometers in the upper troposphere. Thus, we use MM5 (Dudhia, 1993) with a 2-km fine-mesh domain (294-km by 300-km) nested within a 6-km mesh to study a convective event observed on July 23, 2002, during the NASA Cirrus Regional Study of Tropical Anvils and Cirrus Layers – Florida Area Cirrus Experiment (CRYSTAL-FACE). Cumulus parameterization is turned off in both domains and the GSFC 3-ice bulk microphysical scheme is used. The 2-km grid spacing chosen in this study corresponds to a typical grid spacing adopted in cloud resolving models for the GCM super-parameterization approach.

2. CRYSTAL-FACE 23 July 2002 Case

Convection began to form along the east coast of Florida in the early morning between 26 and 27N and then migrated inland. Between 1600 and 2100 UTC, several convective systems with substantial rainfall and area coverage formed around Lake Okeechobee. The anvil generated by these cells subsequently advected across southern Florida and was measured extensively by NASA ER-2, WB-57, and Proteus.

Soundings from Miami, Everglades City and Tampa Bay (from 0000 UTC 23 July to 0000 UTC 24 July) all feature a dry middle troposphere (from 4 to 7 km) and a moist upper troposphere (UT). To further understand the origin of the air masses around Lake Okeechobee, backward trajectories using Hybrid Single-Particle Lagrangian Integrated Trajectory Model (HYSPPLIT, Draxler and Hess, 1997) were performed. The lower tropospheric air (below 2 km) was of maritime origin and came from the southeast. The dust mass concentration for the July 23 case was about $10 \mu\text{g m}^{-3}$, less than the long-term July mean of $16.3 \mu\text{g m}^{-3}$, while the sea salt mass concentration was close to the long-term mean (Sassen et al., 2003). The UT air (9-14 km) was advected from the western United States out over the Atlantic Ocean several hundred of kilometers east of the

Georgia coast, and then turned sharply to the southwest. Persistent convection and associated cloud systems formed off the East Coast between 0700 UTC and 2000 UTC, and likely humidified this UT air. The middle tropospheric air had experienced substantial subsidence in prior days, producing dry conditions.

3. CLOUD SYSTEM SIMULATION

For our study, we used 34 sigma levels up to an altitude of 19.5-km. This gives fairly good vertical resolution in the PBL and a vertical grid spacing of 500-830 m for altitudes between 10 and 15 km. Simulation begins at 0600 UTC 23 July 2002 and continues for 24 hours. The model was initialized using the NCEP 32-km resolution Eta analysis archived on 40-km grids.

Considering the temporal and spatial pattern of the simulated precipitation, the simulation is reasonable. It successfully captures the target convective events, albeit delayed by as much as 2 hours. The principal cirrus outflow direction of the simulated anvil cloud agrees reasonably well with the observations.

A comparison of the simulated hourly cumulative rain contours (10 mm hr^{-1}) with the radar-derived rainmap is shown in Figure 1. We define two adjacent 100-km by 100-km areas (A-1 and A-2). A-2 encloses the target convective events, and A-1 encompasses the trailing anvil system.

The simulated convection in the southwest Florida was overly active. Furthermore, in the simulation, there are a few cells scattered in A-1 as the target convection develops. These cells likely affect the cloud amount and area coverage predicted by the model in A1.

The simulated area mean rainfall rates for A-1 and A-2 also agree reasonably well with the radar-derived values (Figure 2).

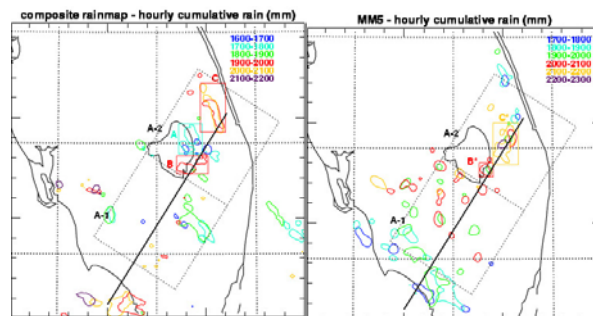


Figure 1. Hourly cumulative rain (10 mm hr^{-1} contour). The solid line indicates aircraft flight path.

* Corresponding author address: David O’C. Starr,
NASA/GSFC, MD, 20771; e-mail:
David.Starr@nasa.gov.

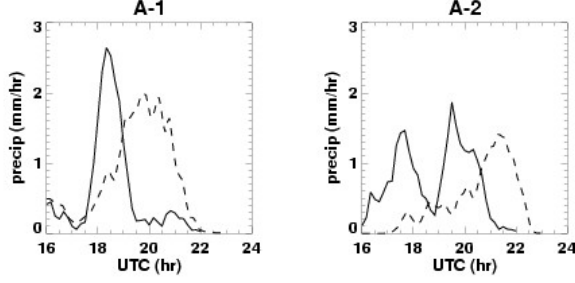


Figure 2. Area mean precipitation rate derived from radar (solid) and MM5 simulation (dashed).

Narrowband outgoing infrared radiation is calculated using a radiative transfer code described in Toon et al (1989) and then compared with the GOES-8 Channel-4 brightness temperature (Figure 3). Although the convection events and precipitation rate are captured reasonably well by the model, the model has generated too much optically thick upper tropospheric clouds, which dissipates much more slowly than observed. The simulated convection might have been more intense and produced higher cloud tops. The simulated anvil base height corresponded well to the observations. This success might be attributed to the persistent and large-scale dry mid-troposphere, which limits the anvil base height for this case.

4. DISSIPATION OF THE SIMULATED ANVIL

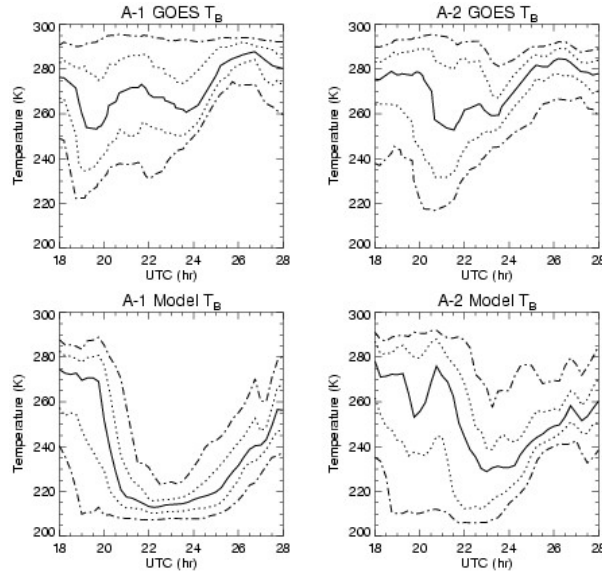


Figure 3. Cumulative probability distribution function of brightness temperature (dashed-dotted, dotted, solid, dotted, dashed-dotted curves are the 10, 30, 50, 70, 90% curves, respectively).

The governing equation for f_i , the total ice water content, $f_i = f_{ci} + f_{sn} + f_{gr}$, in a model grid box is

$$\frac{\partial f_i}{\partial t} + \nabla_H \cdot (f_i \bar{V}_H) + \frac{\partial f_i w}{\partial z} = \frac{\partial f_{ci} V_{t,ci}}{\partial z} + \frac{\partial f_{sn} V_{t,sn}}{\partial z} + \frac{\partial f_{gr} V_{t,gr}}{\partial z} + \rho D + \rho P \quad (1)$$

where V_t is the fall speed, D indicates the summation of the diffusion terms, P is the source/sink term due to phase change, subscripts ci , sn , and gr indicate cloud ice, snow, graupel, respectively. In this case, P due to freezing/melting is negligible in the anvil dissipation phase, especially above $z=8$ -km. We integrate over the two areas respectively (A-1 and A-2) to assess the ice mass budget at GCM grid scale. We partition the integration into the contributions from the area mean fields and eddy terms not resolved by the means. In the following, the overbar is used to denote the area mean.

$$\begin{aligned} \frac{\partial \bar{f}_i}{\partial t} = & \underbrace{-\nabla_H \cdot (f_i \bar{V}_H)}_{\text{HFC}} - \underbrace{\frac{\partial \bar{f}_i w}{\partial z}}_{\text{VFC}_{m,a}} - \underbrace{\frac{\partial w' f_i'}{\partial z}}_{\text{VFC}_{e,a}} \\ & + \underbrace{\frac{\partial [f_{ic} V_{t,ci} + f_{sn} V_{t,sn} (f_{sn}^c) + f_{gr} V_{t,gr} (f_{gr}^c)]}{\partial z}}_{\text{VFC}_{m,s}} \\ & + \underbrace{\left\{ \frac{\partial \bar{f}_{sn} [V_{t,sn} - V_{t,sn} (f_{sn}^c)]}{\partial z} + \frac{\partial \bar{f}_{gr} [V_{t,gr} - V_{t,gr} (f_{gr}^c)]}{\partial z} \right\}}_{\text{VFC}_{e,s}} \\ & + P_m + P_e + \bar{\rho D} \end{aligned} \quad (2)$$

where $\bar{V}_{t,x} = \frac{\int f_x V_{t,x} (f_x) dA}{\int f_x dA}$ (x is sn or gr). Many GCMs

diagnose cloud fraction A_c . Thus, we've incorporated the cloud fraction into some area-mean terms. The overbar superscript c is used to indicate the mean in the cloudy area. Our analysis indicates that the mean ice production may be formulated as

$$P_m = A_c \frac{\bar{\rho w}^c g \left(\frac{1}{C_p} \frac{\partial q_{v,s}(\bar{T})}{\partial T} - \frac{q_{v,s}(\bar{T})}{RT} \right)}{1 + \frac{L}{C_p} \frac{\partial q_{v,s}(\bar{T})}{\partial T}} \quad (3)$$

Such formulation will render a very small eddy production term, P_e .

In the following, we examine the ice mass budget in the anvil dissipation phase, which begins at around 2200 UTC in the simulation.

4.1 Area mean vertical wind

Periods of intense convection are associated with a strong positive \bar{w} from the lower troposphere to the upper troposphere. It is immediately followed by downward \bar{w} in the lower troposphere and upward \bar{w} in the anvil (Figure 4), manifesting the presence of mesoscale updraft and downdraft in the beginning of the

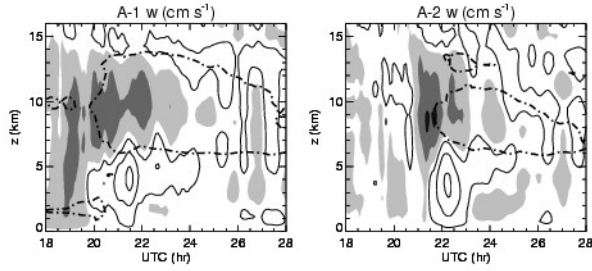


Figure 4. Area mean vertical velocity. Contour levels are -20, -10, -2, 2, 10, 20 cm s^{-1} . Underlines denote filled contours. The dashed contours are $A_c=50\%$.

dissipating stage. As time progresses, \bar{w} weakens and the depth of the positive \bar{w} in the upper anvil shrinks. Above the mid-upper tropospheric mesoscale updraft, is a layer of weak downward \bar{w} , which deepens with time. Note that mesoscale updraft and the weak downward motion atop are not separated by the cloud boundary. The very top of the anvil is within the reign of the weak downward motion. After 2400 UTC, \bar{w} oscillates slowly and weakly across zero.

4.2 Area fraction for different hydrometeor species

The relationship between the cloud fraction and the area fraction of each ice category (cloud ice, snow, and graupel) is not frequently discussed in the literature. We find this relationship a rather interesting issue (Figure 5). As expected, A_c is very close to A_{ci} . The area coverage of graupel is small and reduces to zero in less than 2 hrs due to its fast fall speed and zero production. Graupel is transient, at least for the GCM time step, and perhaps is not crucial in terms of its contribution to the radiation budget. Snow, however, cannot be ignored. The snow category has been incorporated into GCMs (e.g., Fowler et al., 1996). From Figure 5, the area coverage of snow is usually smaller than that of cloud ice. It is expected that the discrepancy, if ignored in GCMs, could introduce bias to the estimated vertical ice mass fluxes.

4.3 Ice mass budget

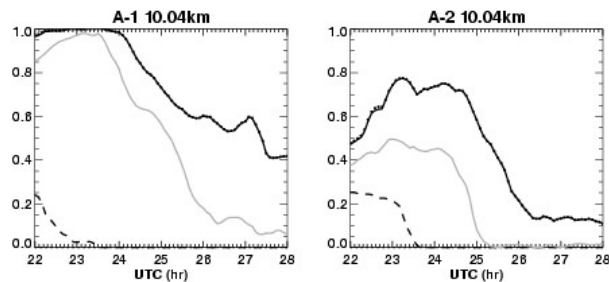


Figure 5. A comparison of the area fraction of ice (solid), snow (gray), and graupel (dashed) at 10.04 km.

The storage term, $\frac{\partial \bar{f}_i}{\partial t}$, is close to the summation of P (production), HFC (horizontal flux convergence), and VFC (vertical flux convergence; the summation of $VFC_{m,a}$, $VFC_{e,a}$, $VFC_{m,s}$, and $VFC_{e,s}$), indicating that $\bar{\rho D}$ is small and negligible with respect to the area mean budget. Once the deep convection has ceased, the storage term is generally negative except when P is large (Figure 6). Its oscillation with time is in phase with that of P . However, P is more important in the mid and lower anvil than the upper level because of the exponential decrease in the saturation vapor pressure with decreasing temperature. HFC is small, but not negligible, and generally negative. VFC is mostly negative and large. The amplitude of the oscillation of VFC is small and the oscillation does not seem to correlate with P . For the selected spatial scale, VFC and P are of comparable magnitude. The anvil base (5 to 7-km) is sublimating during the entire anvil dissipating phase.

4.4 Vertical flux convergence (VFC)

We name VFC_s , that is, VFC due to particle sedimentation, as the summation of $VFC_{m,s}$ and $VFC_{e,s}$ (See equation 1). A similar naming convention is also applied to VFC_a , that is, VFC due to air motion. In general, VFC_s and VFC_a are of the opposite sign. VFC_s is negative in the upper part of the anvil (above

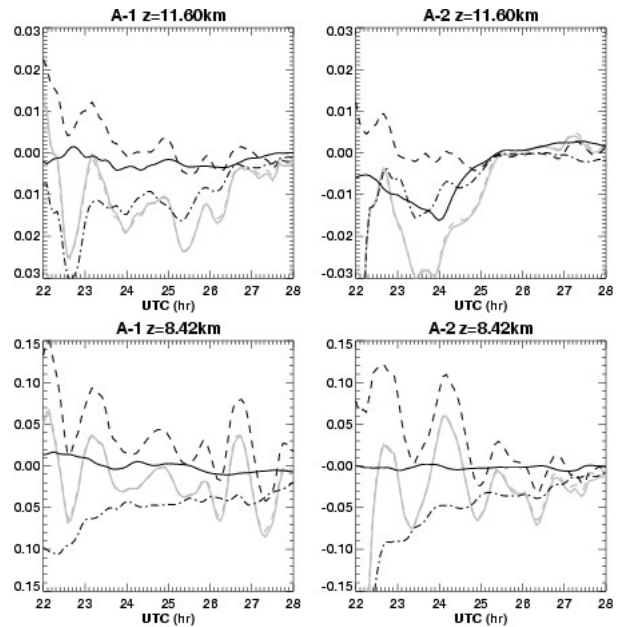


Figure 6. Ice mass budget ($\text{g m}^{-3} \text{hr}^{-1}$) at 2 selected height levels. HFC (solid), VFC (dash-dotted), P (dashed), and the storage term (gray).

z=7-8 km), and positive below. While VFC_s tends to be dominant, VFC_a is not negligible.

Considering a partition into mean state versus eddy contributions, the magnitudes of $VFC_{m,a}$ and $VFC_{e,a}$ are comparable in the beginning. $VFC_{e,a}$ becomes more dominant in the later dissipating phase (after 2530 UTC) as the mean vertical wind weakens.

A GCM with a bulk microphysical scheme estimates the terminal fall speed of the mean particle mass, i.e., $V_{t,sn}(\overline{f_{sn}^c})$, which differs from the grid-by-grid mass weighted fall speed assigned in MM5 which determines the ice mass flux due to particle sedimentation here, i.e., $\overline{V_{t,sn}}$. Thus, $VFC_{e,s}$ is a measure of this difference.

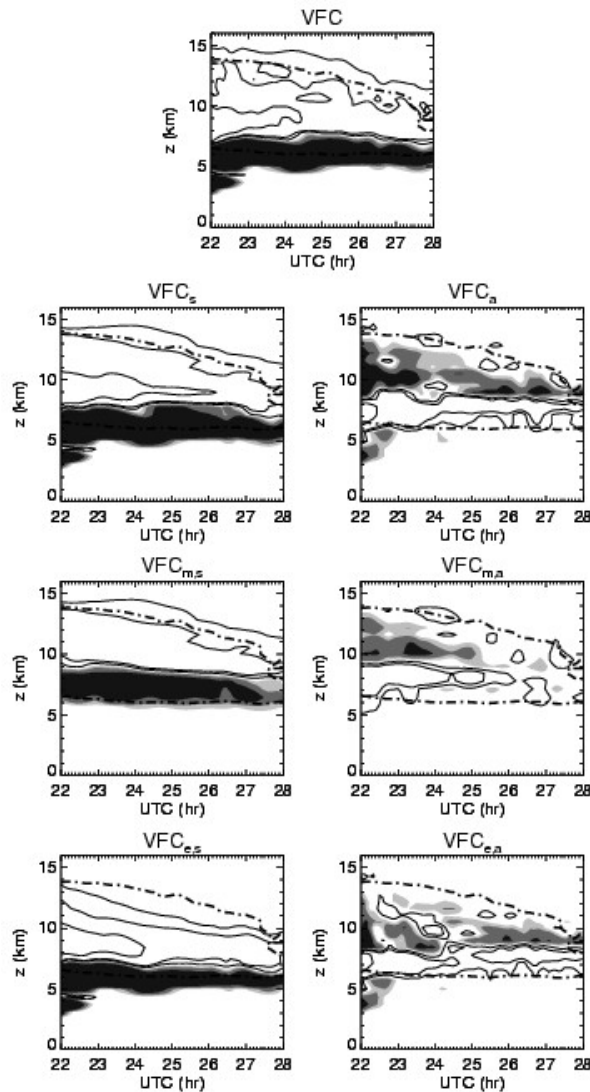


Figure 7. Various vertical flux convergence terms ($\text{g m}^{-3} \text{hr}^{-1}$) in A-1. Contour levels are -0.02, -0.01, -0.005, 0.005, 0.01, 0.02. Underlines denote filled contours.

Fixed terminal speed is prescribed for the cloud ice category in the GSFC 3-ice scheme, and, therefore, cloud ice does not contribute to $VFC_{e,s}$ here. $VFC_{e,s}$ is caused by (1) the non-linear relationship between particle mass and fall speed, and (2) the difference between A_c , A_{sn} , and A_{gr} . As shown in Figure 7, $VFC_{e,s}$ is important in the beginning of the dissipating stage and in the lower anvil, but its impact wanes as the anvil ages and the graupel and snow habits decline.

5. SUMMARY AND OUTLOOK

The dissipating phase of a numerical simulated cirrus anvil is analyzed in details. We integrate the governing equation for the ice mass over a typical grid size (100-km) and examine the contribution of various terms. We find that the effect of cloud scale structure/processes on anvil dissipation cannot be neglected.

This particular simulation, despite capturing the main convection events and overall precipitation successfully, produces a cirrus anvil that is too broad in area coverage, too thick in optical depth, and too slow in dissipation. It is hypothesized that the simulated cumulus flux into the upper troposphere is too large, which indirectly enhances the strength of the mesoscale updraft and result in an anvil system that is more robust than observed. Further examination of the hypothesis will be reported.

ACKNOWLEDGMENTS

The study was supported by NASA Radiation Sciences Program.

REFERENCES

1. Draxler, R. R. and G. D. Hess, 1997: Description of the Hysplit_4 modeling system, NOAA Tech Memo ERL ARL-224, Dec, 24p.
2. Dudhia, J., 1993: A nonhydrostatic version of the Penn State-NCAR Mesoscale Model: Validation tests and simulation of an Atlantic cyclone and cloud front. *Mon. Wea. Rev.*, **121**, 1493-1513.
3. Fowler, L. D., D. A. Randall, and S. A. Rutledge, 1996: Liquid and ice cloud microphysics in the CSU General Circulation Model. Part I: Model description and simulated microphysical processes. *J. Climate*, **9**, 489-529.
4. Sassen, K., P. J. DeMott, J. M. Prospero, and M. R. Poellot, 2003: Saharan dust storms and indirect aerosol effects on clouds: CRYSTAL-FACE results. *Geophys. Res. Lett.*, **30**, doi:10.1029/2003GL017371.
5. Toon, O. B., C. P. McKay, T. P. Ackerman, and K. Santhanam, 1989: Rapid calculation of radiative heating rates and photodissociation rates in inhomogeneous multiple scattering atmospheres, *J. Geophys. Res.*, **94**, 16287-16301.